ACCELERATED PUBLICATION

This paper is available online at www.jbc.org

THE JOURNAL OF BIOLOGICAL CHEMISTRY VOL. 282, NO. 46, pp. 33242–33246, November 16, 2007

Crystallographic Studies of Human MitoNEET*

Received for publication, August 23, 2007, and in revised form, September 24, 2007
Published, JBC Papers in Press, September 27, 2007, DOI 10.1074/jbc.C700172200

Xiaowei Hou[‡§], Rujuan Liu[‡§¶], Stuart Ross[¶‖], Eric J. Smart[‖], Haining Zhu[¶1], and Weimin Gong[‡§2]

From the [‡]National Key Laboratory of Macrobiomolecule, Center for Structural and Molecular Biology, Institute of Biophysics, Chinese Academy of Sciences, Beijing 100101, P. R. China, the [§]School of Life Sciences, University of Science and Technology of China, Hefei, Anhui 230026, P. R. China, the [¶]Department of Molecular and Cellular Biochemistry and the [‖]Kentucky Pediatric Research Institute, Department of Pediatrics, College of Medicine, University of Kentucky, Lexington, Kentucky 40536-0509

MitoNEET was identified as an outer mitochondrial membrane protein that can potentially bind the anti-diabetes drug pioglitazone. The crystal structure of the cytoplasmic mitoNEET (residues 33–108) is determined in this study. The structure presents a novel protein fold and contains a [2Fe-2S] cluster-binding domain. The [2Fe-2S] cluster is coordinated to the protein by Cys-72, Cys-74, Cys-83, and His-87 residues. This coordination is also novel compared with the traditional [2Fe-2S] cluster coordinated by four cysteines or two cysteines and two histidines. The cytoplasmic mitoNEET forms homodimers in solution and in crystal. The dimerization is mainly mediated by hydrophobic interactions as well as hydrogen bonds coordinated by two water molecules binding at the interface. His-87 residue, which plays an important role in the coordination of the [2Fe-2S] cluster, is exposed to the solvent on the dimer surface. It is proposed that mitoNEET dimer may interact with other proteins via the surface residues in close proximity to the [2Fe-2S] cluster.

MitoNEET is a protein recently identified to be localized on the outer membrane of mitochondria (1). It was first identified as a protein cross-linked with photoaffinity probe of pioglitazone, thus appearing to be a pharmacological target of pioglitazone. It was named based on its localization in mitochondria and the Asn-Glu-Glu-Thr (NEET) sequence in its C-terminal domain (2). Pioglitazone is a member of the class of thiazolidinediones (TZDs)[3] that are insulin sensitizers for treatment of type II diabetes (3). It has been shown that pioglitazone functions as a ligand of peroxisome proliferator-activated receptor γ (4). However, additional peroxisome proliferator-activated receptor γ-independent mechanisms have been suggested for the clinical effects of pioglitazone, including its actions on the mitochondrial function (5). Wiley *et al.* (1) recently reported that mitoNEET could negatively regulate electron transport and oxidative capacity of mitochondria since an apparent decrease of the complex I-dependent oxygen consumption was observed in the mitochondria isolated from the mitoNEET-deficient mice heart. Interestingly, pioglitazone was recently reported to have negative regulatory effect on complex I activity in muscle, liver, and astroglioma cells (6, 7) and positive regulatory effect in neuron-like cells (8). This correlation and the mitochondrial localization of mitoNEET suggest that pioglitazone may exert its action on mitochondria by regulating the activities of respiratory complexes via its interaction with mitoNEET.

Type II diabetes is a complex metabolic disease characterized by insulin resistance in the initial stage. The disease and the associated complications have become prevailing public health concerns; thus it is significant to determine the mechanisms by which the anti-diabetes drug pioglitazone functions as an insulin sensitizer. Moreover, it was recently reported that rosiglitazone, another Type II diabetes drug in the thiazolidinedione family that has similar binding affinity to mitoNEET, may increase the risk of myocardial infarction (9, 10). In addition, pioglitazone has also been demonstrated to be a potential treatment of neurodegenerative diseases including multiple sclerosis (11–13), Alzheimer disease (14), and amyotrophic lateral sclerosis (15, 16). Therefore, the structural studies of mitoNEET, which is a potential target of pioglitazone and the TZDs, are highly significant for diabetes and other human diseases.

Here we report the crystal structure at 1.8 Å resolution of the cytoplasmic portion of human mitoNEET (from residues 33–108, referred as mitoNEET$_{33-108}$). The structure of mitoNEET$_{33-108}$ represents a new overall fold and contains a novel Cys_3–His_1 coordinated [2Fe-2S] cluster. The structure reveals a homodimer of mitoNEET$_{33-108}$ with strong hydrophobic interactions and hydrogen bond network at the dimeric interface. The data suggest that it is highly likely that mitoNEET forms a dimer on the outer membrane of mitochondria.

MATERIALS AND METHODS

Protein Expression and Purification—The gene of human mitoNEET$_{33-108}$ was amplified by PCR and cloned to the pMCSG9 vector using the ligation-independent cloning technology (17). His-maltose binding protein-tagged protein was produced in the *Escherichia coli* Rosetta (DE3) strains. Cells were grown at 37 °C in 3.2 liters of LB medium containing 100 μg/ml ampicillin. When A_{600} reached 0.6, the cells were induced at 16 °C for 20 h by adding 0.35 mM isopropyl-β-d-

* This work was supported by the National Funding for Talent Youth Grant 30225015, the Ministry of Science and Technology Grants 2004CB720008, 2006CB0D1705, and 2007CB914304, the 863 program Grant 2006AA02A316, the National Natural Science Foundation of China Grants 10490193 and 30728004 and the Chinese Academy of Sciences Grant KSCX2-YW-R-61 (to W. G.) and by National Institutes of Health Grants R01 DK077632 and P20RR015592 (to E. J. S.) and R01NS049126 (to H. Z.). The costs of publication of this article were defrayed in part by the payment of page charges. This article must therefore be hereby marked "*advertisement*" in accordance with 18 U.S.C. Section 1734 solely to indicate this fact.

The atomic coordinates and structure factors (code 2R13) have been deposited in the Protein Data Bank, Research Collaboratory for Structural Bioinformatics, Rutgers University, New Brunswick, NJ (http://www.rcsb.org/).

[1] To whom correspondence may be addressed: Dept. of Molecular and Cellular Biochemistry, University of Kentucky, 741 South Limestone, Lexington, KY 40536-0509. E-mail: haining@uky.edu.

[2] To whom correspondence may be addressed. E-mail: wgong@ibp.ac.cn.

[3] The abbreviations used are: TZD, thiazolidinedione; PDB, Protein Data Bank; SAD, single anomalous dispersion; MES, 4-morpholineethanesulfonic acid.

thiogalactoside. Then the cells were harvested by centrifugation at 4000 rpm for 30 min. The pellets were resuspended and sonicated in 60 ml of lysis buffer (20 mM Tris-HCl, pH 8.0, 500 mM NaCl). After centrifugation at 16,000 rpm for 30 min, the supernatant was loaded onto a Ni^{2+}-affinity column equilibrated with the lysis buffer. The column was washed sequentially by 20 column volumes of binding buffer (20 mM Tris-HCl, pH 8.0, 20 mM imidazole), and 10 column volumes of washing buffer (20 mM Tris-HCl, pH 8.0, 40 mM imidazole), and then the protein was eluted with elution buffer (200 mM Tris-HCl, pH 8.0, 400 mM imidazole). The eluted solution was cleaved overnight with tobacco etch virus protease at 4 °C, which yields untagged mitoNEET$_{33-108}$ with three residues (Ser-Asn-Ala) at the N terminus. The untagged mitoNEET$_{33-108}$ was further purified by ion-exchange chromatography on a 5-ml HiTrap SP FF ion-exchange column. Fractions containing mitoNEET$_{33-108}$ were desalted and concentrated to ~10 mg/ml in the concentration buffer (20 mM Tris-HCl, pH 8.0) and stored at −20 °C. When being tentatively purified for the first time, the eluted solution after tobacco etch virus protease cleavage was subjected to the size exclusion chromatography before the ion-exchange chromatography, and the retention time suggested that mitoNEET$_{33-108}$ protein existed in solution as a dimer.

Crystallization and Data Collection—Crystals were obtained at 289 K using the hanging-drop vapor diffusion method. Each hanging drop is a 1:1 mixture of protein and reservoir solution. The crystal used for the single anomalous dispersion (SAD) experiment was grown in the reservoir solution containing 2.0 M NaCl and 0.1 M MES, pH 5.5, and the crystal used for the high resolution measurement was grown in the solution containing 2.0 M NaCl and 0.1 M Tris-HCl, pH 9.0. The SAD data set with high redundancy was collected at 100 K on a Rigaku R-AXIS IV++ imaging-plate system with a Rigaku FRE copper rotating-anode generator in Institute of Biophysics, Chinese Academy of Sciences. The data were processed with HKL2000 (18). The high resolution data set was collected at beamline 19ID of the Structural Biology Center at the Advanced Photon Source in the Argonne National Laboratory with the ADSC315 CCD detector and were processed with HKL3000 (19). The processing statistics are summarized in Table 1.

Structure Determination—The crystal structure of human mitoNEET$_{33-108}$ was solved by the SAD method using the anomalous signal of iron atoms. Heavy atom positions were located by SHLXD (20). Heavy atom refinement, phasing, and density flattening were performed by autoSHARP (21). The initial model was automatically built by ARP/wARP (22), manually modified with Coot (23), and refined with Refmac5 (24). The [2Fe-2S] cluster and water molecules were built in according to the $F_o - F_c$ map at the very late stage of refinement. The stereochemical quality of the final model was evaluated by Procheck (25). Structure determination and refinement statistics are listed in Table 1.

RESULTS AND DISCUSSION

Overall Structure—The final model refined to 1.8Å resolution consists of 76 amino acids (Arg-33–Lys-105 of mitoNEET and Ser-Asn-Ala at the N terminus resulting from the vector), one [2Fe-2S] cluster, one chloride ion, and 125 water molecules. Lys-105 was modeled as alanine, and three C-terminal residues (Lys-106, Glu-107, and Thr-108) were not able to be modeled due to the weak electron density. The [2Fe-2S] cluster and chloride ion are identified based on the anomalous difference Fourier map using SAD phases. The $2F_o - F_c$ and difference Fourier map around the [2Fe-2S] cluster and the chloride ion are shown in Fig. 1*A*. The model is well refined, and all the crystallographic data statistics are shown in Table 1.

The structure contains a long loop from Arg-33 to Lys-55 in the N-terminal part and a β-β-α-β topology for the rest of the protein (Fig. 1, *B* and *C*). A [2Fe-2S] cluster is bound in the loop between β2 and α1 and is flanked by the helix α1 and the two-stranded anti-parallel β-sheet (β2β3). The β1 strand is away from the cluster-binding domain (residues from β2 to β3) and interacts with the cluster-binding domain mainly by hydrophobic residues such as Ile-56, Phe-60, Ala-69, Tyr-71, Phe-80, and Phe-82. A structural homology search in the PDB with the program Dali gives two results with the Z-score of 0.5 and 0.4, respectively, indicating that the mitoNEET$_{33-108}$ structure represents a new fold. The secondary structure features are shown in Fig. 1*C*.

In addition, we found two human CDGSH domain-containing proteins (accession numbers A6NMV4 and Q8N5K1) using protein sequence similarity search (blastp on ExPASy against UniProt Knowledgebase). The subcellular localization of Q8N5K1 (named as "Miner 1") was reported (1), but the structure and function of these two proteins are unknown to date. Based on the sequence similarity, we predict that these two proteins are likely to fold similarly as mitoNEET, and the sequence alignment is shown in Fig. 1*C*. In particular, A6NMV4 is a new homolog that has not been reported previously. A6NMV4 has the identical length as mitoNEET and 87% sequence identity with mitoNEET. It remains to be determined whether the new homolog A6NMV4 is a unique protein expressed in human tissues. Its structure and function also need to be elucidated.

[2Fe-2S] Cluster-binding Domain—The [2Fe-2S] cluster is coordinated by Cys-72, Cys-74, and Cys-83 from the loop between β2 and α1 and by His-87 from the start point of α1 (Fig. 1, *B* and *C*). [2Fe-2S] clusters deposited in the PDB heretofore can be classified into two types: four-cysteine coordinated clusters and Rieske clusters with two cysteines and two histidines (Fig. 1*D*). The structure of a [2Fe-2S] cluster coordinated with Cys_3–His_1 as found in this study of mitoNEET is the first time that this novel structure of [2Fe-2S] cluster is demonstrated in crystal structure. Except the coordination residues, the [2Fe-2S] cluster itself is identical to the classical [2Fe-2S] clusters; the two irons and the inorganic sulfurs are in a plane, and the irons are tetrahedrally coordinated (Fig. 1*D*).

The cluster-binding domain of mitoNEET was proposed as a CDGSH-type zinc finger domain based on the sequence information. With the three-dimensional structural determination in this study, we proposed to rename this domain as the third class of [2Fe-2S] cluster-binding domain. In comparison with the consensus motif Cys-X_4-Cys-X_2-Cys-$X_{\approx 30}$-Cys for Cys_4 coordinated [2Fe-2S] clusters in ferredoxins (26) and Cys-*X*-His-X_{15-17}-Cys-X_2-His for Cys_2–His_2 coordinated Rieske [2Fe-2S] cluster (27), the coordinated residues in mitoNEET present an arrangement of Cys-*X*-Cys-X_8-Cys-X_3-His, which results in the unique feature of the [2Fe-2S] cluster-binding domain.

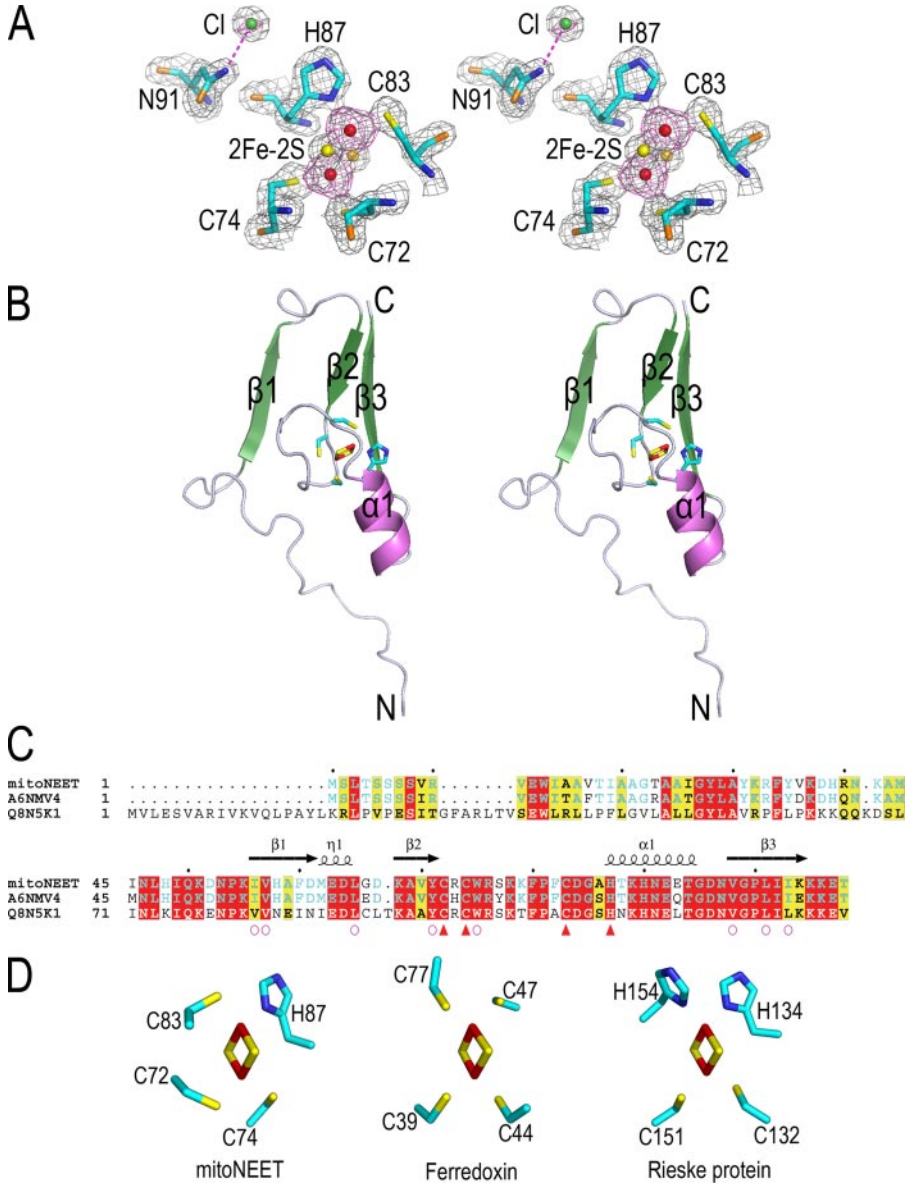

FIGURE 1. **The overall structure and iron-sulfur cluster binding domain of mitoNEET.** *A*, stereo view of the [2Fe-2S] cluster and chloride ion bound to mitoNEET. The $2F_o - F_c$ electron density map (*gray*) is contoured at 1.5 σ. The anomalous difference Fourier density map (*magenta*) is contoured at 4 σ. The [2Fe-2S] cluster and the chloride ion are shown as *spheres* (iron is *red*; sulfur is *yellow*; Chlorine is *green*). The coordinated residues are shown as *sticks* (carbon is *cyan*; nitrogen is *blue*; sulfur is *yellow*; oxygen is *orange*). The *dashed magenta line* indicates the interaction between the chloride ion and the side chain of Asn-91. All images except *panel C* were prepared using the PyMOL program. *B*, ribbon diagram of the overall structure in stereo. The protein is colored by secondary structure elements (α helices are *violet*, β strands are *forest green*, and a single turn of 3_{10} helix is presented as a *loop*) and *numbered* from the N terminus to the C terminus. The [2Fe-2S] cluster and the side chains of the coordinated residues are shown as *sticks* and color-coded as in *panel A*. The three residues (Ser-Asn-Ala) from the expression vector at the N terminus are omitted in all the figures. *C*, the secondary structure of mitoNEET and sequence alignment with two human homologues. The secondary structure features of dimeric mitNEET$_{33-108}$ are shown as defined by DSSP (33). MitoNEET and two human CDGSH domain-containing proteins (A6NMV4 and Q8N5K1) are aligned using clustW (34). The strictly conserved residues are shown in *red boxes*; similar residues are shown in *yellow boxes*. *Red triangles* below the alignment indicate the cluster-coordinated residues, and the *purple circles* indicate the hydrophobic residues involved in dimerization. The residues of mitoNEET are indicated every 10 residues from Met-1 by *black dots* above the alignment. *C* was prepared with ESPript (35). *D*, comparison of [2Fe-2S] clusters from mitoNEET, ferredoxin (PDB code: 1NYK), and Rieske protein (PDB code: 1A70). The [2Fe-2S] cluster and the side chains of the coordinated residues are shown as *sticks* and color-coded as in *panel A*.

These coordinated residues are so close to one another that the loop between β2 and α1 rolls up around the [2Fe-2S] cluster in the cluster-binding domain (Fig. 1*B*). In the open side of the loop, the coordinated residues Cys-83 and His-87 are partially exposed to the polar surroundings, where two water molecules interact respectively with the main-chain oxygen of Cys-83 and the ϵ2 nitrogen of His-87 by hydrogen bonds.

The crystal structure of the [2Fe-2S] cluster is also supported by a recent mitoNEET spectroscopic study that presented spectroscopic evidence suggesting a [2Fe-2S] cluster slightly different from the traditional ones found in ferredoxins and Rieske protein (28, 29). The same study also showed that the [2Fe-2S] cluster coordination to mitoNEET is pH-dependent (28). Our crystal structure of mitoNEET$_{33-108}$ dimer shows that the side chain of His-87 is exposed to solvent and is adjacent to the basic residue Lys-55 from the other monomer (see the discussion on the dimeric structure). Because of the pH dependence of the protonation status of the imidazole ring in histidine and the close proximity of His-87 to a basic residue, our study provides detailed structural support for the reported pH-dependent spectroscopic features.

The Dimeric Structure of mitoNEET—The crystal structure also reveals a homodimer of mitoNEET$_{33-108}$, which is consistent with the retention time on the size exclusion chromatography during protein purification. There is one molecule in an asymmetric unit. A homodimer is formed by the crystallographic 2-fold axis *c* (Fig. 2*A*). Approximately 58% of the hydrophobic residues in mitoNEET$_{33-108}$ exist in the dimer interface, and the dimerization buries 30% of the total surface area in each monomer. The N-terminal β1 strand forms a parallel β sheet with β3 coming from the other monomer. Consequently, two symmetric three-stranded β-sheets are formed face-to-face in the dimer (Fig. 2*A*). Residues such as Val-56 and Val-57 from β1, Leu-65 from the loop between β1 and β2, Tyr-71 from β2, Trp-75 from the loop between β2 and α1, as well as Leu-101 and Ile-103 from β3 provide a number of hydrophobic interactions between the monomers (Fig. 2*B*). Therefore, the dimerization should be very tight and could be necessary for mitoNEET functions. We propose that mitoNEET exists as a dimer under the physiological conditions.

TABLE 1

Data collection, phasing, refinement statistics

Numbers in parentheses correspond to the highest resolution shell.

	SAD	High resolution
Data collection		
Wavelength (Å)	1.5418	0.97937
Space group	$I4_122$	$I4_122$
Unit cell dimensions (Å) and angles (°)	$a = b = 58.959$, $c = 175.231$, $\alpha = \beta = \gamma = 90$	$a = b = 58.794$, $c = 175.306$, $\alpha = \beta = \gamma = 90$
Resolution range (Å)	50–2.3 (2.38–2.30)	30–1.8 (1.86–1.80)
No. of total reflections	320731	336253
No. of unique reflections	7278	14738
Completeness (%)	99.9 (100)	99.4 (99.0)
Redundancy	14.6 (14.8)	9.1 (8.3)
$I/\sigma(I)$	36.21 (9.00)	33.80 (4.78)
R_{merge} (%)[a]	0.123 (0.466)	0.073 (0.440)
Wilson B-factor (Å^2)[b]	33.5	7.2
SAD phasing		
Sites	2	
Resolution (Å)	30-2.3	
Phasing power (anomalous)[c]	0.926	
Structure refinement		
Resolution (Å)		30-1.8
R_{cryst}/R_{free} (%)[d]		15.9/18.8
No. of reflections		
Work set		13189
Test set		699
r.m.s.d.[e] from ideal values		
Bond length (Å)		0.012
Bond angels (°)		1.491
Average B-factor (Å^2)		27.30
No. of atoms		
Protein		627
[2Fe-2S]		4
Chloride ion		1
Waters		125
Ramachandran plot		
Most favored regions (%)		85.1
Additionally allowed (%)		14.9

[a] $R_{merg} = \sum|I_i - I_m|/\sum I_i$, where I_i is the intensity of the measured reflection and I_m is the mean intensity of all symmetry-related reflections.
[b] Wilson B-factor is estimated by Truncate program in CCP4 (36).
[c] Phasing power = $|F_H(\text{calc})|/|E|$, where $F_H(\text{calc})$ is the calculated heavy atom contribution and E is the lack of closure.
[d] $R_{cryst} = \sum||F_{obs}| - |F_{calc}||/\sum|F_{obs}|$, where F_{obs} and F_{calc} are observed and calculated structure factors. $R_{free} = \sum_T||F_{obs}| - |F_{calc}||/\sum_T|F_{obs}|$, where T is a test data set of about 10% of the total reflections randomly chosen and set aside prior to refinement.
[e] r.m.s.d, root mean square deviation.

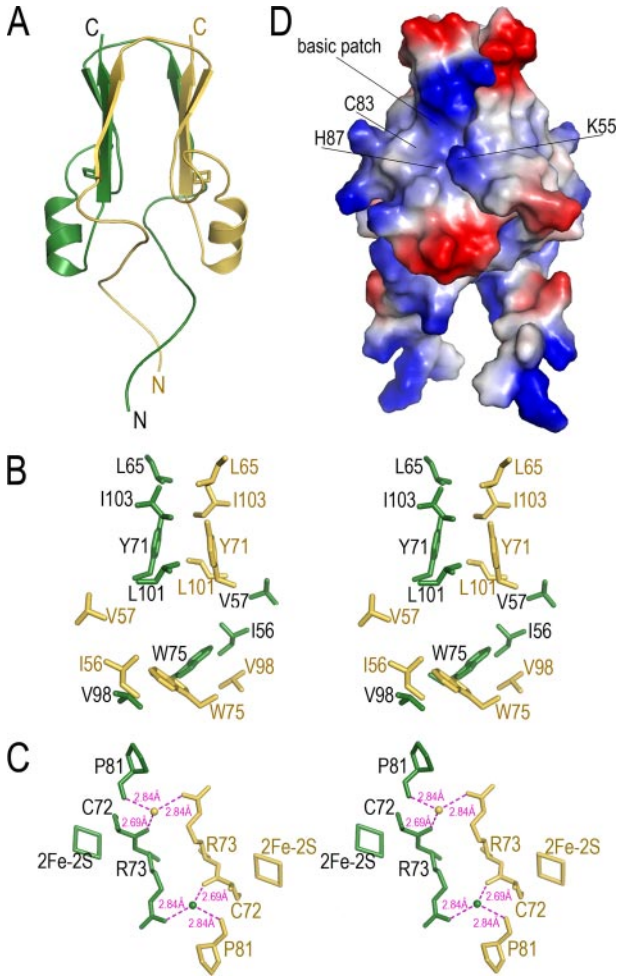

FIGURE 2. **The dimeric structure of mitoNEET.** *A*, ribbon diagram of the mitoNEET$_{33–108}$ dimer. One of the monomers is colored in *forest green*, and the other monomer is colored in *yellow orange*. The *dyad axis* is oriented vertically in the plane of the page. *B*, stereo view of two hydrophobic patches in the dimer interface. The side chains of the hydrophobic residues are shown in *sticks*. The view angle of the left one is the same as in *panel A*, and the residues are colored based on the subunit they belong to in *panel A*. *C*, stereo view of the water molecule at the dimer interface. The residues are shown as *sticks*, and waters are shown as *spheres*. The residues and waters are colored based on the subunit they belong to in *panel A*. The hydrogen bonds between water molecules and the residues are shown as *dashed magenta lines*. The lengths of the hydrogen bonds are shown in the figure. The *dyad axis* is perpendicular to the plane of the page. *D*, surface electrostatic potential map of the mitoNEET$_{33–108}$ dimer. Residues of positive potential are shown in *blue*, and those of negative potential are shown in *red*. The cluster-coordinated residues Cys-83 and His-87 as well as the Lys-55 from the other monomer are indicated. All three residues exist in a basic patch on the surface. The figure is obtained after a 65° anticlockwise rotation around the dyad axis in *panel A* when viewed from the C terminus to the N terminus of the dimer along the axis.

Interestingly, although the dimer interface is mainly hydrophobic, two water molecules are symmetrically buried in the hydrophobic core of the dimer interface. These water molecules link the two monomers by hydrogen bonds with the side chain of Arg-73 and the main-chain oxygen atoms of Pro-81 and cluster-coordinated Cys-72 from the other monomer (Fig. 2*C*). Interfacial water molecules can enhance the stability of protein-protein interactions (30). In the structure of mitoNEET$_{33–108}$ dimer, the two interfacial water molecules make the basic Arg-73 well accommodated to the hydrophobic interface. They also stabilize the two monomers by intermonomer hydrogen bonds. In addition, it is reported that interfacial waters adjacent to redox centers influence their intermolecular electron-transfer reaction (31). In the structure of mitoNEET$_{33–108}$ dimer, the distance of the two clusters is ~14 Å, which is a reasonable distance for potential electron transfer between the two clusters, although the intersubunit electron transfer has not been experimentally tested yet. The structural feature, however, is consistent with the proposed role of mitoNEET in regulating electron transfer reactions in mitochondria (1). Given the special role of Arg-73 in the dimeric interface, we propose that this residue is critical to the structure and function of mitoNEET. We are currently testing this hypothesis by substituting Arg-73 to other residues.

We also solved a mitoNEET$_{33–108}$ structure with a crystal in another space group ($p2_12_12_1$, 3.0 Å resolution, data not shown), in which the same dimer was observed, although the dimer was formed by the non-crystallographic 2-fold symmetry in one asymmetric unit. This structure provides additional support for the observed mitoNEET dimer as representing the physiological dimer.

The N-terminal 32 residues are reported to direct mitoNEET to the outer mitochondrial membrane (1). Using GlobPlot (32),

residues from Trp-13 to Tyr-35 are predicted to constitute a transmembrane domain. In our mitoNEET$_{33-108}$ structure, residues from Ser-33 to Ala-43 are away from the dimerized core. In the dimer, the N terminus of the two monomers extends to the same direction (Fig. 2*A*). It is reasonable to propose that this dimer would exist on the mitochondrial surface with the two N-terminal transmembrane domains inserted into the outer membrane *in vivo*.

The electrostatic surface potential of the dimer is shown in Fig. 2*D*. As discussed earlier, the His-87 residue that is critical to the [2Fe-2S] cluster binding resides in a basic patch on the protein surface. The basic patches on both sides of the dimer may provide a site for interacting with other proteins and small molecules such as pioglitazone. Since the basic patch is in close proximity to the [2Fe-2S] cluster, the binding properties and redox potential of the [2Fe-2S] cluster would be influenced by the proteins and small molecules that can potentially interact with the basic patches.

This study provides critical insights into the structure of mitoNEET and its potential function on the mitochondrial outer membrane. Based on the structure of mitoNEET$_{33-108}$ in this study, it is likely that the binding of pioglitazone or rosiglitazone would significantly change the Fe-S cluster binding and dimeric structure of mitoNEET as well as its function in mitochondria. The structural basis of the interaction between mitoNEET and pioglitazone as well as other TZD compounds is currently under investigation.

Acknowledgments—We thank Yi Han and Dr. Zhijie Liu in the Institute of Biophysics for the SAD diffraction data collection and the high resolution data collection, respectively. The high resolution data were collected at beamline 19ID of the Structural Biology Center at the Advanced Photon Source in the Argonne National Laboratory. The help of Dr. Rongguang Zhang in the data collection and data processing is highly appreciated. The Argonne National Laboratory is operated by the University of Chicago Argonne, LLC, for the U.S. Department of Energy, Office of Biological and Environmental Research under contract DE-AC02-06CH11357.

Addendum—After the submission of this manuscript, two groups published the crystal structure of the cytoplasmic portion of mitoNEET independently (37, 38).

REFERENCES

1. Wiley, S. E., Murphy, A. N., Ross, S. A., van der Geer, P., and Dixon, J. E. (2007) *Proc. Natl. Acad. Sci. U. S. A.* **104,** 5318–5323
2. Colca, J. R., McDonald, W. G., Waldon, D. J., Leone, J. W., Lull, J. M., Bannow, C. A., Lund, E. T., and Mathews, W. R. (2004) *Am. J. Physiol.* **286,** E252–E260
3. Aronoff, S., Rosenblatt, S., Braithwaite, S., Egan, J. W., Mathisen, A. L., and Schneider, R. L. (2000) *Diabetes Care* **23,** 1605–1611
4. Lehmann, J. M., Moore, L. B., Smith-Oliver, T. A., Wilkison, W. O., Willson, T. M., and Kliewer, S. A. (1995) *J. Biol. Chem.* **270,** 12953–12956
5. Feinstein, D. L., Spagnolo, A., Akar, C., Weinberg, G., Murphy, P., Gavrilyuk, V., and Dello Russo, C. (2005) *Biochem. Pharmacol* **70,** 177–188
6. Brunmair, B., Staniek, K., Gras, F., Scharf, N., Althaym, A., Clara, R., Roden, M., Gnaiger, E., Nohl, H., Waldhausl, W., and Furnsinn, C. (2004) *Diabetes* **53,** 1052–1059
7. Perez-Ortiz, J. M., Tranque, P., Burgos, M., Vaquero, C. F., and Llopis, J. (2007) *Mol. Pharmacol.* **72,** 407–417
8. Ghosh, S., Patel, N., Rahn, D., McAllister, J., Sadeghi, S., Horwitz, G., Berry, D., Wang, K. X., and Swerdlow, R. H. (2007) *Mol. Pharmacol.* **71,** 1695–1702
9. Home, P. D., Pocock, S. J., Beck-Nielsen, H., Gomis, R., Hanefeld, M., Jones, N. P., Komajda, M., and McMurray, J. J. (2007) *N. Engl. J. Med.* **357,** 28–38
10. Nissen, S. E., and Wolski, K. (2007) *N. Engl. J. Med.* **356,** 2457–2471
11. Feinstein, D. L., Galea, E., Gavrilyuk, V., Brosnan, C. F., Whitacre, C. C., Dumitrescu-Ozimek, L., Landreth, G. E., Pershadsingh, H. A., Weinberg, G., and Heneka, M. T. (2002) *Ann. Neurol.* **51,** 694–702
12. Pershadsingh, H. A., Heneka, M. T., Saini, R., Amin, N. M., Broeske, D. J., and Feinstein, D. L. (2004) *J. Neuroinflammation* **1,** 3
13. Klotz, L., Schmidt, M., Giese, T., Sastre, M., Knolle, P., Klockgether, T., and Heneka, M. T. (2005) *J. Immunol.* **175,** 4948–4955
14. Heneka, M. T., Sastre, M., Dumitrescu-Ozimek, L., Hanke, A., Dewachter, I., Kuiperi, C., O'Banion, K., Klockgether, T., Van Leuven, F., and Landreth, G. E. (2005) *Brain* **128,** 1442–1453
15. Schutz, B., Reimann, J., Dumitrescu-Ozimek, L., Kappes-Horn, K., Landreth, G. E., Schurmann, B., Zimmer, A., and Heneka, M. T. (2005) *J. Neurosci.* **25,** 7805–7812
16. Kiaei, M., Kipiani, K., Chen, J., Calingasan, N. Y., and Beal, M. F. (2005) *Exp. Neurol.* **191,** 331–336
17. Donnelly, M. I., Zhou, M., Millard, C. S., Clancy, S., Stols, L., Eschenfeldt, W. H., Collart, F. R., and Joachimiak, A. (2006) *Protein Expression Purif.* **47,** 446–454
18. Otwinowski, Z., and Minor, W. (1997) *Methods Enzymol.* **276,** 307–326
19. Minor, W., Cymborowski, M., Otwinowski, Z., and Chruszcz, M. (2006) *Acta Crystallogr. Sect. D Biol. Crystallogr.* **62,** 859–866
20. Schneider, T. R., and Sheldrick, G. M. (2002) *Acta Crystallogr. Sect. D Biol. Crystallogr.* **58,** 1772–1779
21. Vonrhein, C., Blanc, E., Roversi, P., and Bricogne, G. (2006) *Methods Mol. Biol.* **364,** 215–230
22. Perrakis, A., Morris, R., and Lamzin, V. S. (1999) *Nat. Struct. Biol.* **6,** 458–463
23. Emsley, P., and Cowtan, K. (2004) *Acta Crystallogr. Sect. D Biol. Crystallogr.* **60,** 2126–2132
24. Murshudov, G. N., Vagin, A. A., and Dodson, E. J. (1997) *Acta Crystallogr. Sect. D Biol. Crystallogr.* **53,** 240–255
25. Laskowski, R.A., MacArthur, M.W., Moss, D.S., and Thornton, J.M. (1993) *J. Appl. Crystallogr.* **26,** 283–291
26. Lill, R., Dutkiewicz, R., Elsasser, H. P., Hausmann, A., Netz, D. J., Pierik, A. J., Stehling, O., Urzica, E., and Muhlenhoff, U. (2006) *Biochim. Biophys. Acta* **1763,** 652–667
27. Tsoi, T. V., Plotnikova, E. G., Cole, J. R., Guerin, W. F., Bagdasarian, M., and Tiedje, J. M. (1999) *Appl. Environ. Microbiol.* **65,** 2151–2162
28. Wiley, S. E., Paddock, M. L., Abresch, E. C., Gross, L., van der Geer, P., Nechushtai, R., Murphy, A. N., Jennings, P. A., and Dixon, J. E. (2007) *J. Biol. Chem.* **282,** 23745–23749
29. Fee, J. A., Findling, K. L., Yoshida, T., Hille, R., Tarr, G. E., Hearshen, D. O., Dunham, W. R., Day, E. P., Kent, T. A., and Munck, E. (1984) *J. Biol. Chem.* **259,** 124–133
30. Levy, Y., and Onuchic, J. N. (2006) *Annu. Rev. Biophys. Biomol. Struct.* **35,** 389–415
31. Lin, J., Balabin, I. A., and Beratan, D. N. (2005) *Science* **310,** 1311–1313
32. Linding, R., Russell, R. B., Neduva, V., and Gibson, T. J. (2003) *Nucleic Acids Res.* **31,** 3701–3708
33. Kabsch, W., and Sander, C. (1983) *Biopolymers* **22,** 2577–2637
34. Thompson, J. D., Higgins, D. G., and Gibson, T. J. (1994) *Nucleic Acids Res.* **22,** 4673–4680
35. Gouet, P., Courcelle, E., Stuart, D. I., and Metoz, F. (1999) *Bioinformatics (Oxf.)* **15,** 305–308
36. Collaborative Computational Project, Number 4 (1994) *Acta Crystallogr. Sect. D Biol. Crystallogr.* **50,** 760–763
37. Lin, J., Zhou, T., Ye, K., and Wang, J. (2007) *Proc. Natl. Acad. Sci. U. S. A.* **104,** 14640–14645
38. Paddock, M. L., Wiley, S. E., Axelrod, H. L., Cohen, A. E., Roy, M., Abresch, E. C., Capraro, D., Murphy, A. N., Nechushtai, R., Dixon, J. E., and Jennings, P. A. (2007) *Proc. Natl. Acad. Sci. U. S. A.* **104,** 14342–14347